Published in final edited form as:
IEEE Trans Ultrason Ferroelectr Freq Control. 2013 November ; 60(11): 2347–2358. doi:10.1109/TUFFC.2013.6644738.

Harmonic Tracking of Acoustic Radiation Force Induced Displacements

Joshua R. Doherty [Student Member, IEEE], **Jeremy J. Dahl [Member, IEEE]**, and **Gregg E. Trahey [Member, IEEE]**
Department of Biomedical Engineering, Duke University, Durham, NC, 27708 USA

Abstract

Ultrasound-based elasticity imaging methods rely upon accurate estimates of tissue deformation to characterize the mechanical properties of soft tissues. These methods are corrupted by clutter, which can bias and/or increase variance in displacement estimates. Harmonic imaging methods are routinely used for clutter suppression and improved image quality in conventional B-mode ultrasound, but have not been utilized in ultrasound-based elasticity imaging methods. We introduce a novel, fully-sampled pulse inversion harmonic method for tracking tissue displacements that corrects the loss in temporal sampling frequency associated with conventional pulse inversion techniques. The method is implemented with Acoustic Radiation Force Impulse (ARFI) imaging to monitor the displacements induced by an impulsive acoustic radiation force excitation. Custom pulse sequences were implemented on a diagnostic ultrasound scanner to collect spatially-matched fundamental and harmonic information within a single acquisition. B-mode and ARFI images created from fundamental data collected at 4 MHz and 8 MHz are compared with 8 MHz harmonic images created using a bandpass filter approach and the fully sampled pulse inversion method. In homogeneous, tissue-mimicking phantoms, where no visible clutter was observed, there was little difference in the axial displacements, estimated jitter, and normalized cross-correlation among the fundamental and harmonic tracking methods. The similarity of the lower and higher frequency methods suggests that any improvement due to the increased frequency of the harmonic components is negligible. The harmonic tracking methods demonstrated a marked improvement in B-mode and ARFI image quality of *in vivo* carotid arteries. Improved feature detection and decreased variance in estimated displacements were observed in the arterial walls of harmonic ARFI images, especially in the pulse inversion harmonic ARFI images. Within the lumen, the harmonic tracking methods improved the discrimination of the blood–vessel interface, making it easier to visualize plaque boundaries. Improvements in harmonic ARFI images *in vivo* were consistent with suppressed clutter supported by improved contrast and CNR in the matched harmonic B-mode images compared to the fundamental B-mode images. These results suggest that harmonic tracking methods can improve the clinical utility and diagnostic accuracy of ultrasound-based elasticity imaging methods.

I. INTRODUCTION

Diagnostic ultrasound is challenged by the presence of clutter, a noise artifact representing undesirable echoes that interfere with observations made within the region of interest. In B-mode imaging, clutter typically presents as a coherent ring-down artifact or a diffuse haze overlying the image that obscures the visualization of targets and leads to decreased contrast [1]. In Doppler imaging, clutter signals from stationary or slowly moving tissues, such as the vessel walls that are typically 40 to 100 dB stronger than the signal from blood, can

joshua.doherty@duke.edu.

significantly bias blood velocity estimates [2]. Dependent upon the accurate measurement of tissue deformation to characterize the mechanical properties of soft tissues, ultrasound-based elasticity imaging methods are also corrupted by clutter.

Ultrasound-based elasticity imaging methods involve both the excitation of soft tissues and a monitoring of the deformation response. One method, Acoustic Radiation Force Impulse (ARFI) imaging [3, 4], estimates the deformation induced by an impulsive acoustic radiation force excitation to create images that depict the stiffness of structures relative to surrounding tissues [5]. With typical displacements of 1 – 10 μm [6], the presence of stationary clutter can significantly bias ARFI induced tissue displacement estimates. In simulations by Pinton et al. [7], stationary echoes with a −5 dB magnitude relative to moving scatterers resulted in a 24 % underestimation bias of the true 4.8 μm displacement. Clutter imposed bias is commonly observed in vascular ARFI applications [8, 9], where ring-down echoes from the adventitia in blood vessels can corrupt displacements measured in the lumen and make it difficult to delineate the blood–vessel interface and identify plaque boundaries. In addition, clutter can increase the variance in ARFI imaging displacement estimates. This is especially problematic when imaging abdominal structures, such as the liver [10], where high levels of jitter due to near-field reverberation clutter can make it difficult to track the induced deformation. Reduced clutter, therefore, would likely improve the quality and diagnostic accuracy of ARFI imaging.

In Doppler blood flow imaging, wall filters are commonly employed to remove stationary tissue clutter echoes from signals of flowing blood [11]. These methods are less effective for ARFI applications where sufficient spectral separation in the frequency domain is difficult due to significant overlap between the slow ARFI induced tissue velocities (e.g. 10 μm/0.5 msec. = 2 cm/s) and the stationary clutter component. In the time-domain, Gallippi et al. [12] implemented an adaptive blind source separation algorithm to remove physiological vessel wall motion from ARFI induced blood streaming velocities. However, the method has not been shown to reduce clutter in ARFI induced tissue displacement estimates.

In B-mode imaging, tissue harmonic imaging has been shown to reduce clutter and markedly improve image quality [13]. These methods use the harmonics generated as the acoustic wave propagates through soft tissues [14] to create images with improved contrast-to-noise ratio (CNR), finer resolution, lesion visibility, and diagnostic confidence [15-17]. While the specific mechanisms have not been fully described, it has been proposed that harmonic imaging: 1) reduces reverberation clutter from near-field layers, 2) reduces echoes from off-axis scatterers, and 3) is less sensitive to phase aberration [13, 14, 18]. Of these mechanisms, Pinton et al. [1] have recently shown that suppression of reverberation clutter in near-field layers is the dominant source of improvement achieved with harmonic imaging. Despite the benefits demonstrated in B-mode imaging, the use of harmonic imaging has not been adopted in ultrasound-based elasticity imaging methods.

We investigate the use of harmonic methods to track the displacements induced by an impulsive acoustic radiation force excitation. A novel, fully sampled pulse inversion harmonic tracking method is introduced that, unlike conventional pulse inversion methods, does not suffer from a decreased temporal sampling frequency. Performance of this pulse inversion method and a filtered harmonic approach are compared with conventional methods that track the fundamental component of echoes in homogeneous, tissue-mimicking phantoms and *in vivo* carotid arteries.

II. BACKGROUND

A. ARFI Imaging

An ARFI pulse sequence transmits an ensemble of reference pulse(s), pushing pulse(s), and tracking pulse(s) along a single scan line that can be translated across the field-of-view (FOV) to build 2-D or 3-D images. The pushing pulse generates an acoustic radiation force ($\vec{F}$) that is related to the time-average intensity ($\vec{I}$) of the acoustic pulse, the material speed of sound (c), and the absorption coefficient (α) according to (1).

$$\vec{F} = \frac{2\alpha \vec{I}}{c} \quad (1)$$

To generate an appreciable acoustic radiation force, the time-average intensity of the pushing pulse is typically increased by using a higher power and/or longer duration (i.e. 0.1 to 0.5 msec) pulse [6]. To monitor the induced deformation, the reference and tracking pulses are conventional pulse-echo imaging pulses transmitted respectively, before and after, the acoustic radiation force excitation generated by the pushing pulse. Cross-correlation [19] or phase-shift estimation techniques [20, 21] are commonly used to estimate the axial displacement between echoes received by the reference and tracking pulses as a function of time relative to the applied excitation. For a more detailed description of the phenomenon of acoustic radiation force and its utilization in ultrasound-based elasticity imaging methods, the reader is referred to [5].

Ultrasonic tracking methods are susceptible to both jitter and bias displacement errors [22, 23]. Based upon the Cramér-Rao lower bound, a theoretical lower limit of the jitter (σ) can be expressed as (2); where SNR is the signal-to-noise ratio, f_c is the center frequency, T is the correlation window length, B is the fractional bandwidth, and ρ is the correlation value between the signals [24].

$$\sigma \geq \sqrt{\frac{3}{2f_c^3\pi^2 T\,(B^3+12B)}\left(\frac{1}{\rho^2}\left(1+\frac{1}{SNR}\right)^2-1\right)} \quad (2)$$

An inherent underestimation bias of the peak displacement magnitude of tracking methods is primarily due to scatterer shearing, a distortion of the scatterer distribution, within the point spread function of the tracking beam [22, 23].

B. Harmonic Imaging

The propagation of an ultrasonic wave in soft tissue is not a linear process. Nonlinear changes in tissue density result in differences in sound speed during compression and rarefaction of the acoustic wave. This leads to a distortion of the propagating wave and the generation of harmonic frequency components that occur at integer multiples of the fundamental frequency of the transmitted wave [14]. While conventional imaging methods use the fundamental component of returned echoes, tissue harmonic imaging methods create images from these nonlinear harmonics. There are two primary methods to obtain the harmonic components from returned echoes. In the filtered approach, a bandpass filter is used to remove all but the selected harmonic components from the received signal [25]. Alternatively, the pulse inversion (PI) technique transmits two pulses with opposite polarity and then sums their respective echoes [26]. When summed, the linear and odd harmonic components cancel while the even harmonics double [13, 27]. Due to limited transducer bandwidth and because the intensity of the higher order harmonics decrease with increasing

frequency, the second-harmonic is typically used in both of these methods. The doubling of the even harmonic in the pulse inversion method provides an improvement in signal-to-noise ratio (SNR) compared to the filtered approach. In addition, overlap in the spectra of the fundamental and harmonic echoes makes removing the fundamental component, which is typically 10 dB stronger than the second-harmonic component [28], difficult with the filtered approach. Because this overlap increases with the bandwidth of the transmitted pulses, a narrower bandwidth is often required to achieve sufficient separation, such that the filtered harmonic approach involves a trade-off between cancellation of the fundamental echoes and axial resolution [29, 30]. Because it effectively eliminates problems of spectral overlap and can be applied to broadband transmit pulsing, the pulse inversion method is commonly preferred. However, because two pulses must be transmitted to create a single harmonic echo, the frame rate of conventional pulse inversion methods applied in B-mode imaging are reduced by half.

III. FULLY SAMPLED PULSE INVERSION HARMONIC TRACKING

Utilizing the harmonic components to estimate tissue displacements offers several potential advantages. First, (2) predicts decreased jitter with the increased frequency of the harmonic components. Second, the decreased beam width of a higher frequency pulse may also decrease the underestimation bias in measured displacements [22, 23]. In addition, the clutter suppression observed with harmonic methods in conventional B-mode imaging would likely reduce the bias and jitter in displacement estimates from off-axis scatterers and/or reverberation.

Despite potential advantages, the use of harmonic tracking methods for improved displacement estimation is not particularly obvious. Compared to the filtered harmonic approach, (2) predicts a reduction in jitter with the increased SNR of a pulse inversion harmonic technique. However, induced motion that occurs between the acquisition of pulse inverted signals, which are subsequently combined, may reduce correlation between returned echoes and thereby increase jitter. In addition, the decreased temporal sampling frequency of conventional pulse inversion methods may be particularly challenging for tracking the transient response of soft tissue to an impulsive acoustic radiation force excitation. With a decreased temporal resolution, it is more difficult to capture the peak displacement of the tissue response. While the specific results of this effect depend upon material properties, such as shear wave speed, a decrease in measured displacement may result in decreased contrast if the magnitude of the measured displacement approaches the jitter magnitude [31].

To increase the temporal sampling frequency, a fully sampled (i.e. no loss in temporal resolution) pulse inversion summing scheme demonstrated in Fig. 1 is proposed. Here, pulses of opposite polarity are alternately transmitted at a pulse repetition frequency (PRF) equal to $1/t_{prf}$, where t_{prf} is the pulse repetition time between subsequent transmits, to track the arbitrary displacement recovery curve in Fig. 1a. In this idealized ARFI deformation response the axial displacements are monitored for a period that begins before the excitation is applied and extends for a duration beyond the peak displacement response. As shown in Fig. 1b, the conventional pulse inversion method results in a temporal sampling frequency that is half the PRF of the transmitted pulses. By combining returned echoes with alternate pairs of pulse inverted echoes, the fully sampled pulse inversion method shown in Fig. 1c can be used to create a harmonic dataset with a temporal sampling frequency equal to the PRF of the transmitted pulses.

IV. METHODS

A. Pulse Sequencing

Custom pulse sequences were developed that acquire spatially-matched fundamental B-mode, fundamental ARFI, harmonic B-mode, and harmonic ARFI information within a single acquisition. As shown in Fig. 2, the ARFI pulse sequence consisted of two portions. In the first portion of the sequence, an ensemble of 4 MHz pulses that alternate in polarity was transmitted to monitor the deformation response at each of several spatially-distinct lateral locations. In the second portion of the sequence, an ensemble of 8 MHz fundamental pulses of identical polarity was transmitted at each of the same lateral locations that were used in the first portion of the sequence. As indicated, multiple images can be created from the echoes received using this pulse sequence, including: 1) 4 MHz fundamental, 2) filtered harmonic, and 3) pulse inversion harmonic, all from the first portion of the sequence, and 4) 8 MHz fundamental data from the second portion of the sequence.

A 4 MHz 150 μsec pushing pulse with an F/3 configuration was used in both portions of the sequence. The deformation response was monitored 0.7 msec before and 2.6 msec following the start of the acoustic radiation force excitation at a PRF of 9.4 kHz using a single on-axis (i.e. aligned with the center of the applied excitation) tracking beam. The excitation and tracking beam ensemble was applied at 50 distinct lateral locations uniformly distributed across a 15 mm FOV. The total duration of the pulse sequence was 420 msec. The pulse sequences were implemented on a diagnostic ACUSON S2000™ ultrasound scanner with a 9L4 linear array transducer (Siemens Medical Solutions USA, Inc., Issaquah, WA).

B. Data Acquisition

Data were acquired in calibrated, tissue-mimicking, elastic, homogeneous phantoms (CIRS Corporation, Norfolk, VA) with Young's Modulus (E) values of 4.5 kPa, 9 kPa, and 24 kPa, as determined by the manufacturer using an indenter system. In the phantoms, data were separately acquired at focal depths of 20 mm and 30 mm.

Data were also acquired *in vivo* in the carotid artery of human subjects according to an Institutional Review Board approved protocol (Duke University Protocol ID: Pro00012795). All subjects provided written, informed consent prior to participation in the study. The study population included normal, healthy subjects with no known carotid artery plaques and subjects with carotid artery plaques that had been previously identified during a routine ultrasound exam. For each subject, between three and five imaging data sets were acquired at multiple imaging locations, with a few second pause between acquisitions, to confirm spatial and temporal repeatability of the images.

In phantom and *in vivo* experiments, raw radiofrequency data were acquired at 40 MHz and processed off-line with MATLAB™ (The MathWorks, Natick, MA) software.

C. Data & Image Processing

The pulse inversion transmit scheme used in the first portion of the pulse sequence (Fig. 2) results in a halving of the temporal sampling frequency between returned echoes of identical polarity. To create the fully sampled 4 MHz fundamental data, the returned echoes of alternating polarity were separately tracked with respect to their own reference pulse, and then combined.

The harmonic components of the received radiofrequency data were obtained using both the filtered and pulse inversion approaches. In the filtered approach, a 50-tap FIR bandpass filter centered at 8 MHz with a fractional bandwidth of 0.3 was applied to the fully sampled 4

MHz data to obtain the second-harmonic components. The pulse inversion harmonic ARFI data was created using the fully sampled pulse inversion harmonic method (Fig. 1c). Created from 4 MHz transmits, the 8 MHz (i.e. second-harmonic) components are most dominant in the pulse inversion harmonic data.

The summing of two echoes separated in time, as performed in the fully sampled pulse inversion harmonic approach (Fig. 1), may function as a low-pass filter. To evaluate the impact of this potential averaging effect, 8 MHz fundamental radiofrequency data was summed according to the fully sampled pulse inversion harmonic approach to create averaged 8 MHz fundamental data. Because the polarity of the summed 8 MHz fundamental echoes are identical, no fundamental cancellation occurs.

Axial displacement estimates were calculated using normalized cross-correlation (NCC) with a 1.5λ tracking kernel that was updated for the different frequencies between the fundamental and harmonic methods [32]. In the homogeneous phantom experiments, outliers in the raw displacement estimates were removed by discarding estimates greater than the 95th percentile of the displacements measured at each depth and time following the start of the acoustic radiation force excitation. For *in vivo* data, quadratic motion filters were used to remove artifacts from non-ARFI induced motion such as physiologic and transducer motion [33]. Unless otherwise stated, all ARFI images and corresponding displacement and normalized cross-correlation values represent estimates 0.80 msec after the start of the acoustic radiation force excitation. This specific time was chosen empirically because it was approximately the time in which maximum contrast was observed in all ARFI images.

The ARFI images and displacements reported herein correspond to the absolute magnitude of the estimated displacements. Previous studies have reported positive and negative, high magnitude displacement noise within the lumen of blood vessels in ARFI images [9]. Absolute magnitude images show improved visualization of the blood by reducing this spatially-variant noise within the lumen. Because negative displacements are not observed outside the lumen, depicting the absolute magnitude of the displacements does not affect the visualization of the soft tissue regions.

D. Data Analysis

For each ARFI acquisition (i), the axial displacement ($\delta_{i,j,k}$) and associated normalized cross-correlation value ($\rho_{i,j,k}$) were estimated at each axial depth (j) and lateral location (k). In the homogeneous phantoms, the mean displacement ($\bar{\delta}_{i,j}$) and mean normalized cross-correlation value ($\bar{\rho}_{i,j}$), across all $N = 50$ lateral locations, were determined according to (3) and (4), respectively. Because the true displacement is unknown, the mean displacement ($\bar{\delta}_{i,j}$) was used to estimate the jitter ($\psi_{i,j}$), the root-mean-square of the displacement error, for each phantom acquisition according to (5) [22].

$$\bar{\delta}_{i,j}=\frac{1}{N}\sum_{k=1}^{N}\delta_{i,k,j} \quad (3)$$

$$\bar{\rho}_{i,j}=\frac{1}{N}\sum_{k=1}^{N}\rho_{i,k,j} \quad (4)$$

$$\psi_{i,j}=\sqrt{\frac{1}{N}\sum_{k=1}^{N}\left(\delta_{i,j,k}-\bar{\delta}_{i,j}\right)^2} \quad (5)$$

To compare the performance of the tracking methods in phantoms, we report the mean and standard deviation of the 1) mean displacement ($\bar{\delta}_{i,j}$), 2) jitter estimate ($\psi_{i,j}$), and 3) mean normalized cross-correlation coefficient ($\bar{\rho}_{i,j}$) value from ten independent acquisitions obtained at different spatial locations within the phantom for each tracking method.

Measurements of the mean and standard deviation of the measured axial displacements and normalized cross-correlation values within the carotid artery wall of a normal, healthy subject are used to compare the tracking methods *in vivo*. In the presence of carotid artery plaques, which are known to be heterogeneous structures [34], variance in the displacement may actually correspond to different materials, such as lipid pools, intraplaque hemorrhage, and/or calcifications, within the arterial wall. For this reason, in the presence of carotid artery plaques, improvements will only be characterized on the basis of feature detection and qualitative improvements.

Contrast (6) and contrast-to-noise ratio (CNR) (7) were measured to quantify B-mode image quality according to:

$$\text{Contrast}=-20\ \log_{10}\left(\frac{S_i}{S_0}\right) \quad (6)$$

$$CNR=\frac{|S_i-S_0|}{\sqrt{\sigma_i^2+\sigma_0^2}} \quad (7)$$

Here, S_i and S_o represent the mean signal magnitudes inside and outside the region of interest, respectively, and σ_i^2 and σ_0^2 are the corresponding variances. For each image shown, the lumen and adjacent arterial walls were manually segmented to define the inside and outside regions, respectively. To preserve image clarity, the boundaries of these regions have not been identified in the images shown.

V. RESULTS

A. Phantom Imaging

Fig. 3 compares the mean axial displacement, jitter estimate, and mean normalized cross-correlation among the fundamental and harmonic tracking methods in an E = 9 kPa homogeneous, elastic, tissue-mimicking ultrasound phantom with a focal depth of 30 mm. The solid lines correspond to the mean value with shaded error bars representing one standard deviation across ten independent acquisitions. In some cases, especially for the mean displacement, the small magnitude of the error bars makes them difficult to visualize. In Fig. 3a the tracking methods are compared as a function of axial depth at a fixed time of 0.8 msec following the start of the acoustic radiation force excitation. Conversely, in Fig. 3b, the methods are compared as a function of time following the start of the acoustic radiation force excitation at a fixed depth of 30 mm. The mean displacements are nearly identical for all tracking methods through depth (Fig. 3a) and time (Fig. 3b). Differences between the jitter estimates for the various tracking methods depend upon the specific time and depth,

but are relatively small in magnitude for all cases. For most times and depths, the 4 MHz fundamental method has the largest normalized cross-correlation value, followed by the nearly identical 8 MHz fundamental and filtered harmonic methods, with the pulse inversion harmonic method having the lowest normalized cross-correlation value. However, at the focal depth of 30 mm and at a time shortly following the peak displacement response, which is usually represented in an ARFI image, the normalized cross-correlation value of all methods is quite similar and in all cases is greater than 0.993. As a function of time following the start of the acoustic radiation force excitation, there is a subtle oscillation of the mean displacement, jitter estimate, and normalized cross-correlation values for the 4 MHz fundamental, filtered harmonic, and pulse inversion harmonic data sets created from the pulse inverted echoes (Fig. 3b). Similar small differences between the tracking methods demonstrated in this particular configuration were observed in phantoms of stiffnesses E = 4.5 kPa and E = 24 kPa and at focal depths of 20 mm and 30 mm, but the results have been omitted for conciseness.

B. In Vivo Imaging

Fig. 4 shows matched B-mode and ARFI images of a carotid artery (CA) and jugular vein (JV) in a normal, healthy subject. Qualitatively, less clutter is observed within the lumen of the carotid artery in the harmonic B-mode images (Fig. 4c-d) compared to the fundamental B-mode images (Fig. 4a-b). This observation is consistent with contrast values of 21.42 dB, 22.88 dB, 25.03 dB, and 28.61 dB and CNR values of 0.97, 0.71, 1.01, and 0.95 that were measured in the 4 MHz fundamental, 8 MHz fundamental, filtered harmonic, and pulse inversion harmonic B-mode images respectively. In the jugular vein, a bright, coherent signal, indicated by the yellow arrows, is observed in the 4 MHz fundamental B-mode image (Fig. 4a). This apparent clutter signal is also observed in the 8 MHz fundamental B-mode image (Fig. 4b), but less so in the filtered harmonic B-mode image (Fig. 4c), and barely noticeable in the pulse inversion harmonic B-mode image (Fig. 4d). The narrow bandpass filter that was necessary to remove this artifact in the filtered harmonic B-mode image (Fig. 4c) appears to have degraded the axial resolution. Overall, there is a marked improvement in the delineation of the blood–vessel interfaces along the proximal and distal walls, where they appear smoother in the harmonic B-mode images (Fig. 4c-d). In particular, the boundary of the intima with the lumen in the distal wall is more clearly resolved in the pulse inversion harmonic B-mode image (Fig. 4d).

In the ARFI images, because the applied acoustic radiation force magnitude is dependent upon focal and absorption effects, the key information portrayed is the relative displacement of a region of interest compared to that of surrounding tissues. In general, the stiff vessel walls have uniform displacement of low magnitude (i.e. less than 1 μm) compared to the softer, surrounding tissues with higher displacements. Relatively high magnitude displacement noise exists within the lumen of the ARFI images and is greatest in the harmonic ARFI images, particularly in the pulse inversion harmonic ARFI image (Fig. 4d).

In the 4 MHz fundamental and 8 MHz fundamental ARFI images (Fig. 4a-b), the proximal wall of the carotid artery is difficult to distinguish from surrounding tissues and the lumen of the jugular vein. A marked improvement in visualization of the proximal wall is demonstrated in the harmonic ARFI images, most notably with the pulse inversion harmonic ARFI image (Fig. 4d). In addition, the boundaries of the distal wall are much smoother in the pulse inversion harmonic ARFI image compared to the other ARFI images.

The bright, coherent clutter signal observed in the B-mode image presents as a region of increased displacement greater than 3 μm within the jugular vein near the proximal wall of the carotid artery, indicated by the yellow arrows, in the matched 4 MHz fundamental ARFI image (Fig. 4a). Similar to the trend observed in the B-mode amplitude, this region of

increased displacement is also observed in the 8 MHz fundamental ARFI image (Fig. 4a), but is reduced in the filtered harmonic ARFI image (Fig. 4c), and is least obvious in the pulse inversion harmonic ARFI image (Fig. 4d).

Measurements of the mean displacement and mean normalized cross-correlation values plus and minus one standard deviation within the proximal wall, distal wall, and lumen of the carotid artery portrayed in Fig. 4 are listed in Table I for each ARFI image. The location of the measurement regions, which were based upon the pulse inversion harmonic ARFI image, are indicated by the white-dashed contours in Fig. 4a. Estimates of the ARFI induced tissue displacements are of reduced magnitude and have less variance in the distal wall in the harmonic ARFI images (Table I). This is especially true for the pulse inversion harmonic ARFI image, which also has the lowest displacement variance in the proximal wall. In the lumen, the magnitude and standard deviation of the axial displacement is significantly greater in the harmonic ARFI images and is greatest in the pulse inversion harmonic ARFI image. The normalized cross-correlation values are quite similar within the proximal and distal walls for all tracking methods. In the lumen, however, the normalized cross-correlation value in the harmonic ARFI images are significantly reduced in magnitude and have greater variance, especially in the pulse inversion harmonic ARFI image.

Fig. 5 shows matched B-mode and ARFI images of a carotid artery and jugular vein in a subject with known carotid artery plaques. For conciseness, only the 8 MHz fundamental and pulse inversion harmonic images are portrayed. In the B-mode images, the plaque boundaries are better visualized in the pulse inversion harmonic image (Fig. 5b) compared to the fundamental image (Fig. 5a). Despite similar contrast values of 18.93 dB and 19.04 dB, this qualitative comparison is consistent with the improved CNR value of 1.20 compared to 0.93 for the pulse inversion harmonic and 8 MHz fundamental B-mode images, respectively.

In the pulse inversion harmonic ARFI image (Fig. 5b) there is improved delineation of the blood–vessel interface at the proximal and distal walls of the jugular vein compared to the 8 MHz fundamental ARFI image (Fig. 5a). Within the carotid artery, the magnitude of displacements in the narrow region of the lumen is similar in magnitude to the displacements in the adjacent plaque and arterial wall regions in the 8 MHz fundamental ARFI image (Fig. 5a), making it difficult to visualize the lumen and identify plaque boundaries. The greater displacements observed within the lumen of the carotid artery in the pulse inversion harmonic ARFI image (Fig. 5b) improve the discrimination of blood from soft tissues and makes it easier to visualized the plaque boundaries.

Improved feature detection within the plaques is achieved with the pulse inversion harmonic tracking method. To better illustrate this, an expanded view of the region of interest indicated by the solid white lines has been provided for the ARFI images in Fig. 5a-b. In these expanded views, a region of increased displacement that is approximately 2 μm within the distal wall carotid plaque, indicated by yellow arrows, can be seen in the pulse inversion harmonic ARFI image (Fig. 5b). This particular feature is not readily identified in the 8 MHz fundamental ARFI image (Fig. 5a), but is spatially registered with a hypoechoic region of similar geometry that can be seen in both the fundamental and pulse inversion harmonic B-mode images.

Fig. 6 shows matched B-mode and ARFI, 8 MHz fundamental and pulse inversion harmonic images acquired at the bifurcation of a carotid artery in a subject with a small plaque on the distal wall. Regions of low correlation in the ARFI images have been masked by setting displacement values with a normalized cross-correlation value less than 0.97 to black.

Within the lumen of the carotid artery in the pulse inversion harmonic B-mode image (Fig. 6b), there is suppressed clutter compared to the 8 MHz fundamental B-mode image (Fig. 6a). The pulse inversion harmonic method demonstrates significant improvements in contrast and CNR; 20.84 dB contrast and 1.35 CNR for the pulse inversion harmonic B-mode image compared to 16.31 dB contrast and 0.77 CNR for the 8 MHz fundamental B-mode image.

The reduced normalized cross-correlation values associated with displacement estimates in regions of blood demonstrated by the pulse inversion harmonic ARFI images (Table I) allow for improved discrimination of blood from regions of soft tissue. With the correlation threshold in Fig. 6, the blood–vessel interfaces along the proximal and distal walls of the carotid artery are more clearly delineated in the pulse inversion harmonic ARFI image (Fig. 6b) compared to the 8 MHz fundamental ARFI image (Fig. 6a). In addition, the correlation threshold removed displacement noise from the jugular vein in the pulse inversion harmonic ARFI image (Fig. 6b) that cannot be identified in the 8 MHz fundamental ARFI image (Fig. 6a).

Fig. 7 shows ARFI images for the averaged 8 MHz fundamental data collected in the subjects shown previously in a) Fig. 4, b) Fig. 5, and c) Fig. 6. As previously described, this averaged data was created by summing the identical polarity 8 MHz fundamental radiofrequency data according to the fully sampled pulse inversion harmonic approach (Fig. 1c) developed herein. In comparing the non-averaged and averaged 8 MHz fundamental ARFI images (Fig. 4b with Fig. 7a, Fig. 5a with Fig. 7b, and Fig. 6a with Fig. 7c) no noticeable difference is observed.

VI. DISCUSSION

Despite the extensive use of tissue harmonic imaging in conventional ultrasound, to the best of our knowledge the utilization of harmonic tracking methods for ultrasound-based elasticity imaging has not been reported in the literature. As mentioned previously, theoretical improvements associated with the increased frequency of the harmonic components include: 1) decreased jitter based upon the Cramér-Rao lower bound and 2) reduced underestimation bias associated with a smaller tracking beam size [22, 23]. In addition, it seems likely that harmonic methods, which have been shown to suppress clutter in B-mode imaging [13], may also reduce clutter imposed bias and jitter errors in tissue displacement estimates. Towards realizing such benefits, we developed a novel pulse inversion harmonic method with an improved temporal sampling frequency to monitor the transient deformation from an impulsive acoustic radiation force excitation. In phantoms and *in vivo* experiments, we compared this pulse inversion harmonic tracking method with a filtered harmonic approach and conventional techniques that use the fundamental component of returned echoes to form a displacement estimate.

In the phantom experiments (Fig. 3) the jitter increased and normalized cross-correlation decreased with increasing displacement magnitude, which is consistent with ARFI imaging simulations and experiments reported by others [22, 23]. We suspect subtle differences in the pulse inverted transmit signals, due to nonlinearities in the ultrasound system, are responsible for the slight oscillation observed through time (Fig. 3b) in the 4 MHz fundamental, filtered harmonic, and pulse inversion harmonic datasets created from the pulse inverted echoes. Despite this small artifact, the relatively smooth profiles observed through time (Fig. 3b) demonstrate how the fully sampled pulse inversion harmonic method (Fig. 1c) can be used to reliably track the transient deformation response without a degraded temporal sampling frequency. The slight decrease in normalized cross-correlation values observed with the pulse inversion harmonic method (Fig. 3) is likely due to motion that

occurs between pulse inverted transmits. The small magnitude of this decorrelation seems reasonable given the relatively small displacements and does not appear to increase jitter. For the various focal depths and phantom stiffnesses investigated in this study, any difference in the harmonic and fundamental tracking methods appear to be independent of shear wave speeds and focal effects.

No visible clutter was observed in the homogeneous phantoms used in this study such that no improvement due to clutter suppression associated with the harmonic methods was expected in the phantom experiments. This can explain the similarity between the 8 MHz fundamental method with the 8 MHz filtered and pulse inversion harmonic methods. In addition, the similarity of the higher frequency tracking methods (filtered harmonic, pulse inversion harmonic, and 8 MHz fundamental) compared to the lower frequency 4 MHz fundamental tracking method in phantoms suggests that improvements, if any, due to an increased frequency are also insignificant. Similar results were observed in simulations by Palmeri et al. [22], who demonstrated that an increased tracking frequency can reduce bias and jitter only if the transducers fractional bandwidth, centered about the tracking frequency, is held constant with increasing tracking frequency. This would require the absolute bandwidth to scale proportionately with the increasing frequency. The fixed bandwidth about the center frequency of our transducer likely explains why the theoretical improvements predicted by the Cramér-Rao lower bound (2) were not observed. Without clutter and with no improvements due to increased tracking frequency, the similarity between the harmonic and fundamental tracking methods observed in the phantoms is not surprising. Despite the lack of improvement shown in the homogeneous phantoms, these results indicate that any improvement observed with harmonic tracking methods in a more challenging environment, such as *in vivo* imaging, cannot be attributed to increased tracking frequency and are likely due to suppressed clutter.

The use of harmonic tracking methods markedly improved the quality of *in vivo* ARFI imaging. In general, an improved sensitivity to discriminate blood from soft tissues, making it easier to detect the blood–vessel interface, and improved visualization of arterial features was demonstrated in the harmonic ARFI images compared to the fundamental ARFI images in Fig. 4, Fig. 5, and Fig. 6. The comparison between averaged 8 MHz fundamental ARFI images (Fig. 7) with the non-averaged 8 MHz fundamental ARFI images (Fig. 4b, Fig. 5a, and Fig. 6a), suggests that the low-pass filter effect from the summation of pulses temporally separated is negligible. These results also suggest that the improvements observed in the pulse inversion harmonic images are not attributed to a simple averaging effect. The reduced clutter observed in the harmonic B-mode images, supported by improved contrast and CNR, suggests that the improvements observed in the harmonic ARFI images *in vivo* are also due to a reduction in clutter.

Clutter suppression achieved with harmonic tracking methods is also supported by differences in the measured displacements and associated normalized cross-correlation values between the fundamental and harmonic ARFI images (Table I). It has been well described in Doppler literature that clutter from stationary or slowly moving tissues can result in an underestimation of the measured blood velocities [2]. Removal of clutter signals would therefore reduce this bias and lead to an increase in the measured displacements of the blood. In addition, because stationary clutter is significantly more correlated and of higher intensity than echoes from flowing blood, the removal of clutter signals would lead to decreased normalized cross-correlation values and subsequently, according to (2), increased displacement variance within the lumen. The increased displacement magnitude, decreased normalized cross-correlation, and increased displacement variance demonstrated in the lumen of Fig. 4 (Table I) with the harmonic ARFI images, especially the pulse inversion harmonic ARFI image (Fig. 4d), are therefore, all indicative of reduced bias associated with

the removal of stationary or slowly moving clutter. Similar arguments can also explain the increased displacement in Fig. 5b and the decreased normalized cross-correlation in Fig. 6b within the lumen for the pulse inversion harmonic ARFI images.

We suspect the decreased B-mode amplitude and decreased ARFI displacement observed in the harmonic images near the proximal wall in the jugular vein in Fig. 4 are due to a suppression of clutter. While the specific source is unknown, this region presents as a large, bright echo, representative of ring-down reverberation in the 4 MHz fundamental B-mode image. In the spatially-matched ARFI image, this artifact presents as a region of increased displacement that we suspect is biased by clutter from overlying tissues. The near removal of this clutter signal in the harmonic images, especially in the pulse inversion harmonic images, suggests that harmonic tracking methods are less susceptible to such artifacts. We also suspect reduced biasvia suppression of diffuse clutter to account for the improved visualization of the small region of increased displacement within the distal wall plaque in the pulse inversion harmonic ARFI image in Fig. 5b. With the hypoechoic region of similar spatial location and geometry observed in both the fundamental and harmonic B-mode images of Fig. 5, we believe this region is in fact a structural feature of the plaque and not an imaging artifact. Improved visualization of such small features are promising for ARFI imaging methods aimed at differentiating carotid plaques containing small, soft lipid pools believed to be more vulnerable from more stable, calcified plaques [9, 35]. In addition to reduced bias, the decreased variance in displacements measured within the stiff arterial walls of the harmonic ARFI images in Fig. 4 (Table I) measured in the pulse inversion harmonic ARFI image suggests harmonic tracking may also reduce jitter in displacement estimates.

While the improvements demonstrated *in vivo* are consistent with a removal of clutter, the specific mechanisms are somewhat unclear. Unfortunately, clutter generating phantoms do not exist commercially and reliably generating clutter in a controlled experiment remains a challenge. In addition, while recent methods allow for simulating the nonlinear propagation of waves and can account for multiple reflections and scattering [36], these methods do not allow for investigating small micron-size ARFI displacements. For these reasons, we are currently limited to the *in vivo* demonstration of harmonic tracking provided herein. Nonetheless, because the 4 MHz fundamental, filtered harmonic, and pulse inversion harmonic images were created from the same radiofrequency data, with the 8 MHz fundamental acquisition occurring 210 msec later in time (Fig. 2), it seems unlikely that any *in vivo* motion could account for the demonstrated improvements. In addition, while not explicitly shown, the improvements in harmonic image quality *in vivo* were consistent across multiple acquisitions and scanning locations separated in time, such that the images were temporally and spatially stable.

The improvements demonstrated with the harmonic tracking methods *in vivo*, especially with the fully sampled pulse inversion harmonic approach, are promising. It seems likely that other ARFI applications, including cardiac and abdominal imaging, where large amounts of clutter from near-field reverberation are known to degrade B-mode image quality, would also benefit from the reduced bias and jitter of harmonic tracking methods. The improved estimation of soft tissue displacements may also provide more accurate estimates of wave velocity for acoustic radiation force shear wave based methods that track the off-axis deformation response to quantify material properties. While the pulse inversion harmonic method seems particularly well suited for the relatively small displacements associated with acoustic radiation force based elasticity imaging methods, the method may also find use in other ultrasound-based elasticity imaging methods such as strain imaging and elastography [37].

VII. CONCLUSIONS

The utility of harmonic imaging methods for improved ARFI imaging was evaluated. We developed a novel pulse inversion harmonic tracking method with an improved temporal sampling frequency to monitor the transient deformation induced by an impulsive acoustic radiation force excitation. In phantoms, little difference was observed between fundamental and harmonic tracking methods to suggest that improvements associated with the increased tracking frequency of the harmonic components was negligible. Significant improvements were demonstrated *in vivo* and were consistent with a reduction of clutter. In particular, the pulse inverted harmonic tracking method reduced bias from clutter within the lumen of vessels for improved discrimination of blood and arterial boundaries and reduced jitter within the arterial walls for improved feature detection.

Acknowledgments

The authors would like to thank Siemens Medical Solutions USA, Inc., Ultrasound Division for their in-kind technical support.

This work was supported by NIH grants R01HL075485 and R37HL096023 from the NHLBI.

REFERENCES

[1]. Pinton GF, Trahey GE, Dahl JJ. Sources of Image Degradation in Fundamental and Harmonic Ultrasound Imaging: A Nonlinear, Full-Wave, Simulation Study. IEEE Trans Ultrason Ferroelect Freq Contr. 2011; 58(6):1272–1283.

[2]. Bjaerum S, Torp H, Kristoffersen K. Clutter filters adapted to tissue motion in ultrasound color flow imaging. IEEE Trans Ultrason Ferroelect Freq Contr. Jun; 2002 49(6):693–704.

[3]. Nightingale KR, Palmeri ML, Nightingale RW, Trahey GE. On the Feasibility of Remote Palpation Using Acoustic Radiation Force. J Acoust Soc Am. 2001; 110(1):625–634. [PubMed: 11508987]

[4]. Nightingale K, Soo MS, Nightingale RW, Trahey GE. Acoustic radiation force impulse imaging: in vivo demonstration of clinical feasibility. Ultrasound Med Biol. 2002; 28(2):227–235. [PubMed: 11937286]

[5]. Doherty JR, Trahey GE, Nightingale KR, Palmeri ML. Acoustic Radiation Force Elasticity Imaging in Diagnostic Ultrasound. IEEE Trans Ultrason Ferroelect Freq Contr. 2013; 60(4):685–701.

[6]. Nightingale KR. Acoustic radiation force impulse (ARFI) imaging: A review. Current Medical Imaging Review. 2011; 7(4):328–339.

[7]. Pinton GF, Dahl JJ, Trahey GE. Rapid tracking of small displacements with ultrasound. IEEE Trans Ultrason Ferroelect Freq Contr. 2006; 53(6)

[8]. Trahey GE, Palmeri ML, Bentley RC, Nightingale KR. Acoustic radiation force impulse imaging of the mechanical properties of arteries: in vivo and ex vivo results. Ultrasound Med Biol. Sep; 2004 30(9):1163–1171. [PubMed: 15550320]

[9]. Dahl JJ, Dumont DM, Allen JD, Miller EM, Trahey GE. Acoustic radiation force impulse imaging for noninvasive characterization of carotid artery atherosclerotic plaques: a feasibility study. Ultrasound Med Biol. 2009; 35(5):707–716. [PubMed: 19243877]

[10]. Fahey BJ, Nelson RC, Bradway DP, Hsu SJ, Dumont DM, Trahey GE. In vivo visualization of abdominal malignancies with acoustic radiation force elastography. Phys Med Biol. 2008; 53:279–293. [PubMed: 18182703]

[11]. Jensen, JA. Estimation of blood velocities using ultrasound. Cambridge University Press; 1996.

[12]. Gallippi CM, Nightingale KR, Trahey GE. BSS-based filtering of physiological and ARFI-induced tissue and blood motion. Ultrasound in Medicine & Biology. Nov.2003 29(11):1583–1592. [PubMed: 14654154]

[13]. Tranquart F, Grenier N, Eder V, Pourcelot L. Clinical Use of Ultrasound Tissue Harmonic Imaging. Ultrasound in Medicine & Biology. 1999; 25(6):889–894. [PubMed: 10461715]

[14]. Humphrey VF. Nonlinear propagation in ultrasonic fields: measurements, modelling and harmonic imaging. Ultrasonics. Mar.2000 38(1-8):267–72. [PubMed: 10829672]

[15]. Choudhry S, Gorman B, Charboneau JW, Tradup DJ, Beck RJ, Kofler JM, Groth DS. Comparison of tissue harmonic imaging with conventional US in abdominal disease. Radiographics : a review publication of the Radiological Society of North America, Inc. 2000; 20(4):1127–35.

[16]. Desser TS, Jeffrey RB, Lane MJ, Ralls PW. Tissue harmonic imaging: utility in abdominal and pelvic sonography. Journal of clinical ultrasound. 1998; 27(3):135–42. [PubMed: 10064411]

[17]. Kornbluth M, Liang DH, Paloma A, Schnittger I. Native tissue harmonic imaging improves endocardial border definition and visualization of cardiac structures. Journal of the American Society of Echocardiography. Jul; 1998 11(7):693–701. [PubMed: 9692526]

[18]. Thomas JD, Rubin DN. Tissue harmonic imaging: why does it work? Journal of the American Society of Echocardiography. Aug.1998 11(8):803–8. [PubMed: 9719092]

[19]. Embree, P. Ph.D. dissertation. University of Illinois; Urbana, Ill.: 1985. The accurate ultrasonic measurement of the volume flow of blood by time-domain correlation.

[20]. Kasai C, Namekawa K, Koyano A, Omoto R. Real-time two-dimensional blood flow imaging using an autocorrelation technique. IEEE Trans Ultrason Ferroelect Freq Contr. 1985; SU-32(3): 458–464.

[21]. Loupas T, Powers J, Gill R. An axial velocity estimator for ultrasound blood flow imaging, based on a full evaluation of the doppler equation by means of a two-dimensional autocorrelation approach. IEEE Trans Ultrason Ferroelect Freq Contr. 1995; 42(4):672–688.

[22]. Palmeri ML, McAleavey SA, Trahey GE, Nightingale KR. Ultrasonic tracking of acoustic radiation force-induced displacements in homogeneous media. IEEE Trans Ultrason Ferroelectr Freq Control. Jul; 2006 53(7):1300–1313. [PubMed: 16889337]

[23]. McAleavey SA, Nightingale KR, Trahey GE. Estimates of echo correlation and measurement bias in acoustic radiation force impulse imaging. IEEE Trans Ultrason Ferroelect Freq Contr. 2003; 50(6):631–641.

[24]. Walker WF, Trahey GE. A fundamental limit on delay estimation using partially correlated speckle signals. IEEE Trans Ultrason Ferroelect Freq Contr. 1995; 42(2):301–308.

[25]. Christopher T. Finite Amplitude Distortion-Based Inhomogeneous Pulse Echo Ultrasonic Imaging. IEEE Trans. Ultrason.,Ferroelec.,Freq. Contr. 1997; 44(1):125–139.

[26]. Chapman, CS.; Lazenby, JC. Ultrasound Imaging System Employing Phase Inversion Subtraction to Enhance the Image. U.S. Patent 5,632,277. May 27. 1997

[27]. Ma Q, Ma Y, Gong X, Zhang D. Improvement of tissue harmonic imaging using the pulse-inversion technique. Ultrasound in medicine & biology. Jul; 2005 31(7):889–94. [PubMed: 15972194]

[28]. Cobbold, RS. Foundations of Biomedical Ultrasound. Oxford University Press; New York, NY: 2007.

[29]. Simpson DH, Chin CT, Burns PN. Pulse inversion Doppler: a new method for detecting nonlinear echoes from microbubble contrast agents. IEEE Trans Ultrason Ferroelect Freq Contr. Jan.1999 46(2):372–82.

[30]. Morgan KE, Allen JS, Dayton P. a. Chomas JE, Klibaov a. L. Ferrara KW. Experimental and theoretical evaluation of microbubble behavior: effect of transmitted phase and bubble size. IEEE Trans Ultrason Ferroelect Freq Contr. Jan.2000 47(6):1494–509.

[31]. Nightingale KR, Palmeri ML, Trahey GE. Analysis of contrast in images generated with transient acoustic radiation force. Ultrasound Med Biol. Jan.2006 32(1):61–72. [PubMed: 16364798]

[32]. Bonnefous O, Pesque P. Time Domain Formulation of Pulse-Doppler Ultrasound and Blood Velocity Estimation by Cross Correlation. Ultrasonic Imaging. 1986; 8:73–85. [PubMed: 2946098]

[33]. Hsu SJ, Bouchard RR, Dumont DM, Wolf PD, Trahey GE. In vivo assessment of myocardial stiffness with acoustic radiation force impulse imaging. Ultrasound Med Biol. Nov.2007 33(11): 1706–1719. [PubMed: 17698282]

[34]. Hellings WE, Peeters W, Moll FL, Piers SRD, van Setten J, Van der Spek PJ, de Vries J-PPM, Seldenrijk K. a. De Bruin PC, Vink A, Velema E, de Kleijn DPV, Pasterkamp G. Composition of carotid atherosclerotic plaque is associated with cardiovascular outcome: a prognostic study. Circulation. May; 2010 121(17):1941–50. [PubMed: 20404256]

[35]. Doherty JR, Dumont DM, Trahey GE, Palmeri ML. Acoustic radiation force impulse imaging of vulnerable plaques: a finite element method parametric analysis. Journal of Biomechanics. Nov. 2013 46:83–90. [PubMed: 23122224]

[36]. Pinton GF, Dahl JJ, Rosenzweig SJ, Trahey GE. A heterogeneous nonlinear attenuating full-wave model of ultrasound. IEEE Trans. Ultrason.,Ferroelec.,Freq. Contr. 2009; 56(3):474–488.

[37]. Ophir J, Cespedes I, Ponnekanti H, Yazdi Y, Li X. Elastography: a quantitative method for imaging the elasticity of biological tissues. Ultrasonic Imaging. 1991; 13(2):111–134. [PubMed: 1858217]

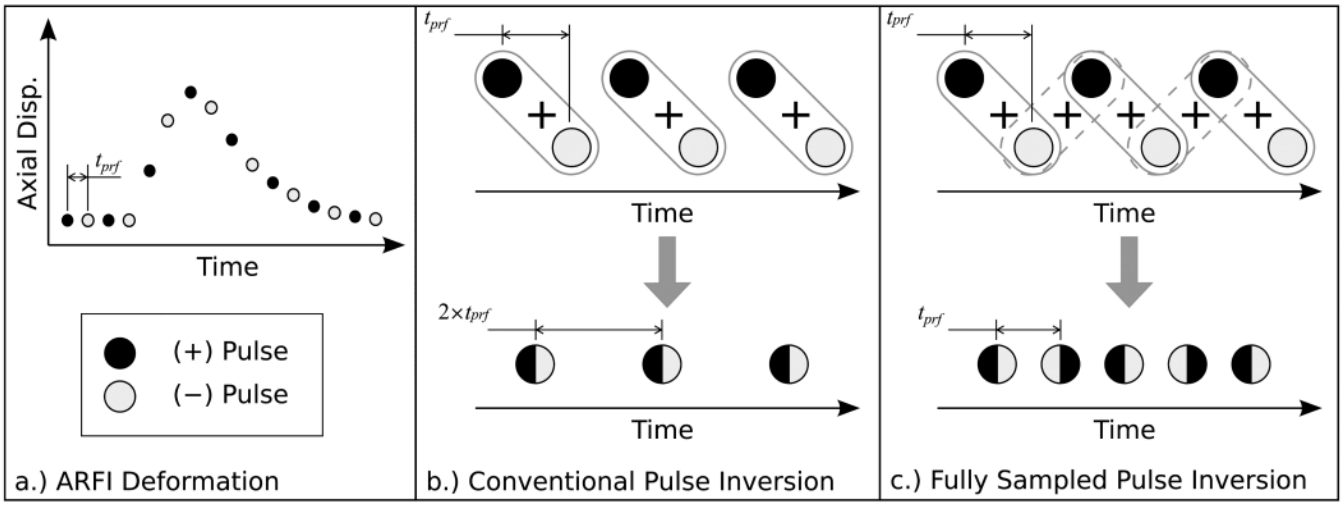

Fig. 1.

a) Arbitrary ARFI deformation response that is monitored using a pulse inversion scheme that transmits pulses of alternating polarity (+ and −) at a PRF equal to $1/t_{prf}$, where t_{prf} is the pulse repetition time between subsequent transmits. As shown, the response is monitored for a period that begins before the excitation and extends for a duration beyond the peak displacement response. b) The conventional pulse inversion method sums each (+) pulse with the subsequent (−) pulse, resulting in a temporal sampling frequency of $1/(2 \times t_{prf})$. c) The proposed fully sampled pulse inversion method sums each (+) pulse with the subsequent (−) pulse, but also sums each (−) pulse with the subsequent (+) pulse to construct a harmonic signal with a temporal sampling frequency of $1/t_{prf}$, which is equal to the PRF of the transmitted pulses.

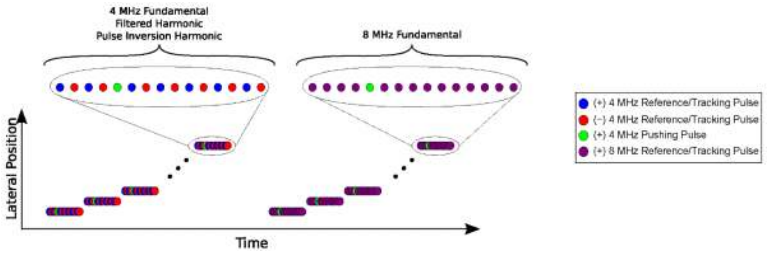

Fig. 2.

ARFI pulse sequence consisting of an ensemble of reference pulse(s), pushing pulse(s), and tracking pulse(s) applied at each of multiple lateral locations uniformly distributed across the FOV. In the first portion of the sequence, 4 MHz pulse inverted (+ and −) pulses were used to construct 1) 4 MHz fundamental 2) filtered harmonic and 3) pulse inversion harmonic images. In the second portion of the sequence, identical polarity (+) 8 MHz pulses were used to construct an 8 MHz fundamental image.

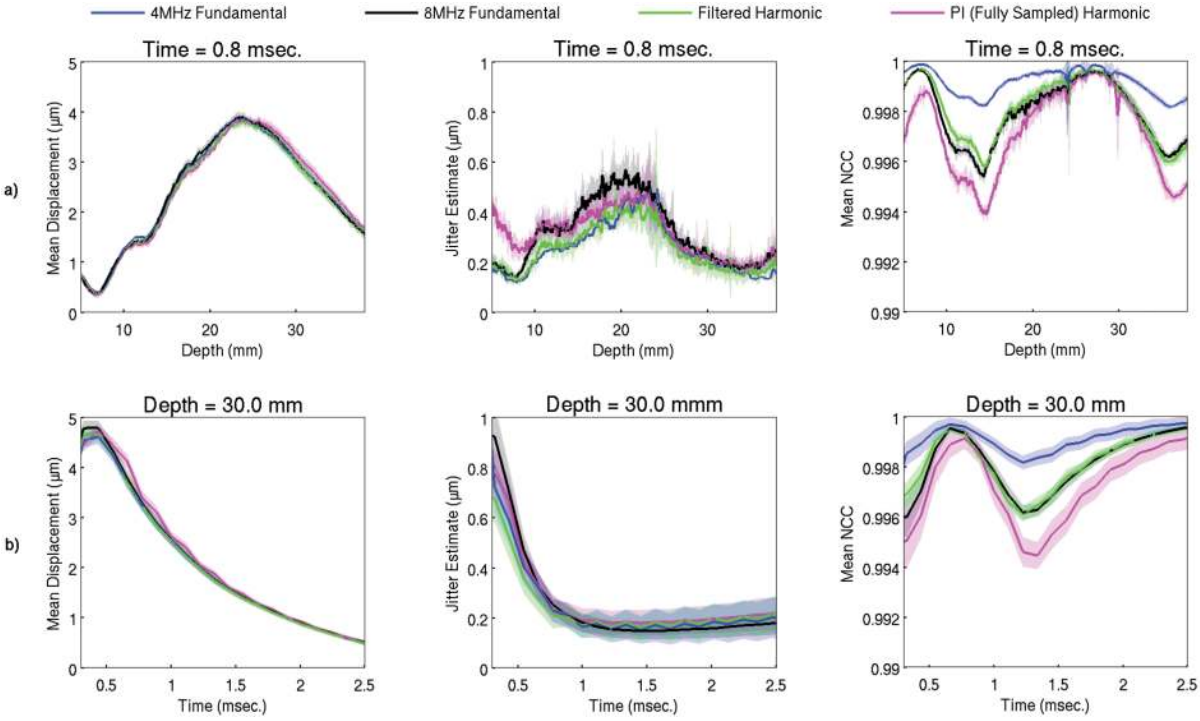

Fig. 3.

The mean axial displacement, jitter estimate, and mean normalized cross-correlation (NCC) profiles among the fundamental and harmonic tracking methods acquired in an $E = 9$ kPa homogeneous, elastic, tissue-mimicking ultrasound phantom with a focal depth of 30 mm. The solid lines correspond to the mean value with shaded error bars representing one standard deviation across ten independent acquisitions recorded at different locations within the phantom. In a) the tracking methods are compared as a function of depth at 0.8 msec following the start of the acoustic radiation force excitation. In b) the tracking methods are compared as a function of time following the start of the acoustic radiation force excitation at a depth of 30 mm.

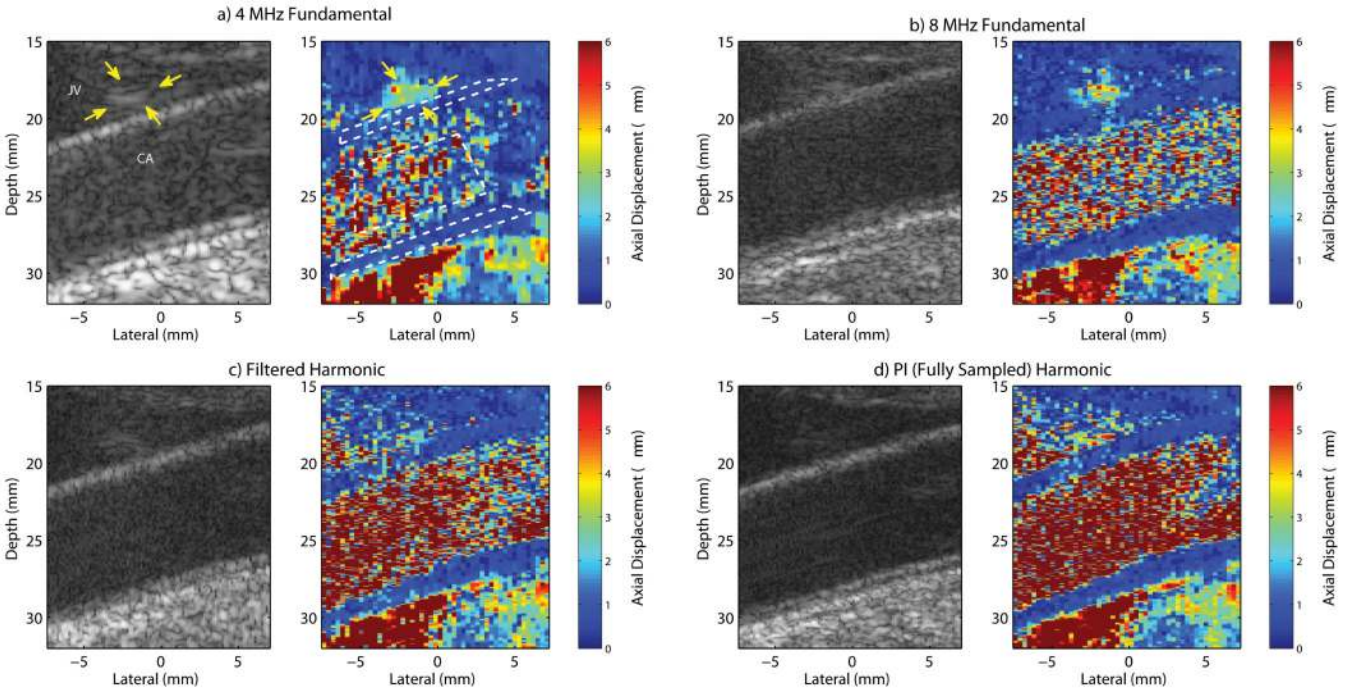

Fig. 4.

In vivo a) 4 MHz fundamental, b) 8 MHz fundamental, c) filtered harmonic, and d) fully sampled pulse inversion (PI) harmonic B-mode and ARFI images of a carotid artery (CA) and jugular vein (JV) in a healthy, normal subject. Yellow arrows in the 4 MHz fundamental images indicate a spatially-matched region of increased B-mode amplitude and increased ARFI displacement within the jugular vein near the proximal wall. The white-dashed contours in the 4 MHz fundamental ARFI image indicate the regions corresponding to the measured displacements and normalized cross-correlation values listed in Table I.

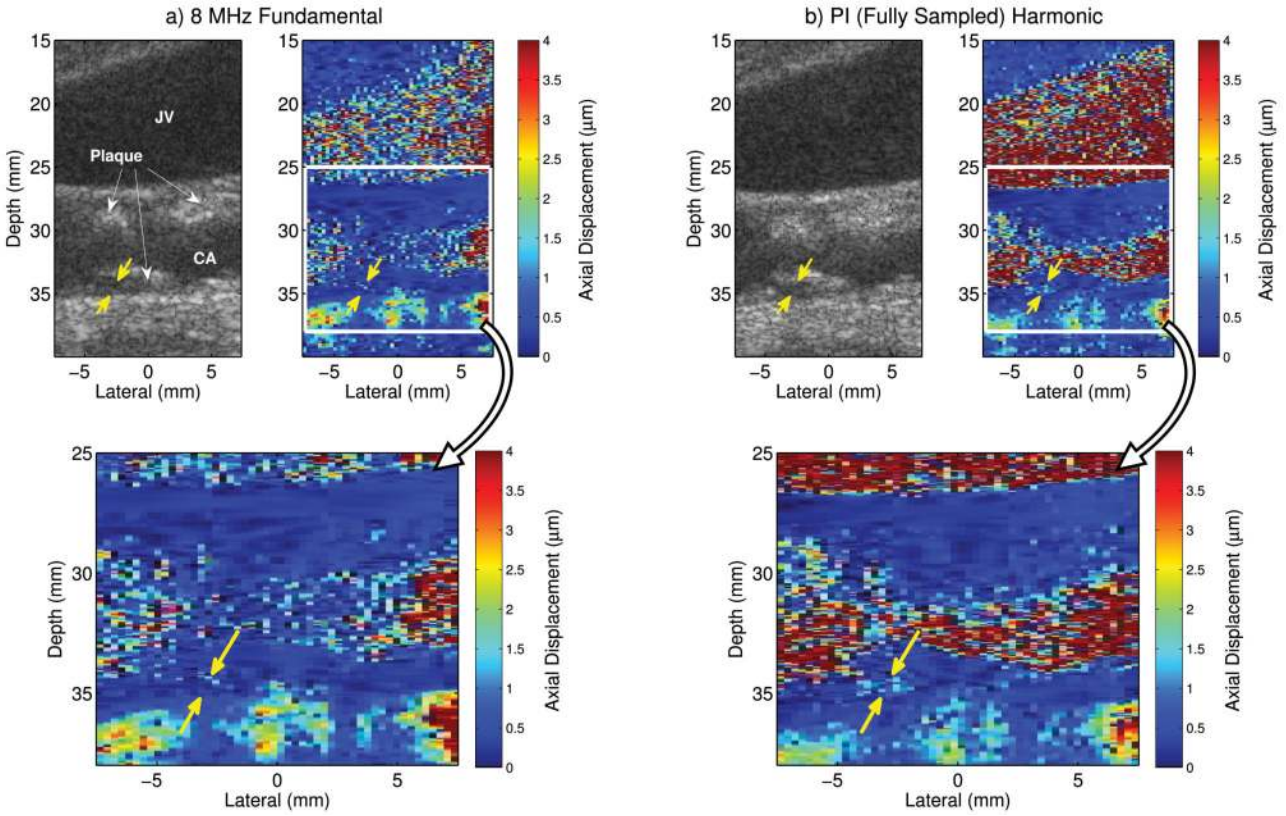

Fig. 5.

In vivo a) 8 MHz fundamental and b) fully sampled pulse inversion (PI) harmonic B-mode and ARFI images of a carotid artery (CA) and jugular vein (JV) in a subject with known carotid artery plaques. The region of interest indicated by the solid-white lines in the ARFI images are shown enlarged for each method. Yellow arrows indicate a region of increased displacement that is approximately 2 μm in the pulse inversion harmonic ARFI image that spatially registers to a hypoechoic region of similar geometry in the B-mode images.

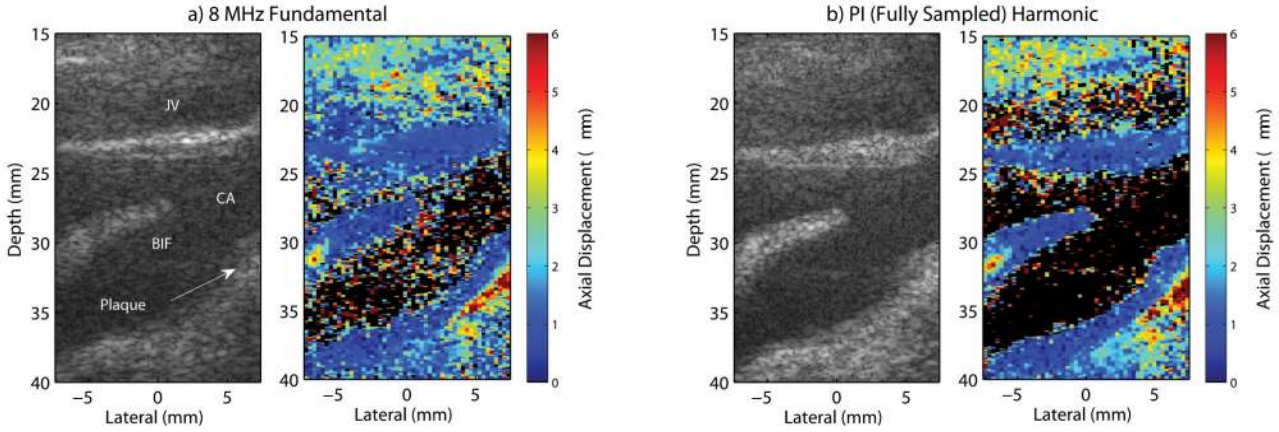

Fig. 6.

In vivo a) 8 MHz fundamental and b) fully sampled pulse inversion (PI) harmonic B-mode and ARFI images showing the bifurcation (BIF) of the carotid artery (CA) with the shallower jugular vein (JV) in a subject with known carotid artery plaques. Displacements with a normalized cross-correlation value less than 0.97 have been set to black.

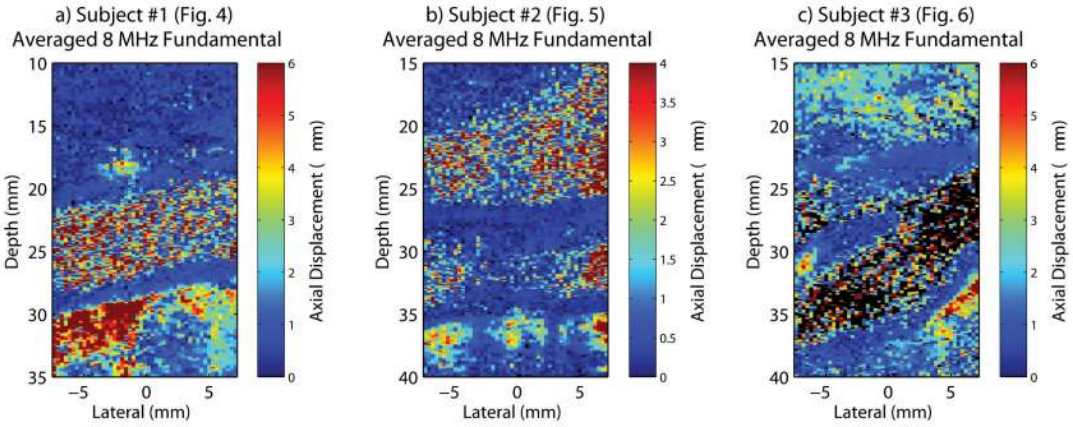

Fig. 7.

In vivo averaged 8 MHz fundamental ARFI images obtained in subjects previously shown in a) Fig. 4, b) Fig. 5, and c) Fig. 6.

TABLE I

Axial Displacement Estimates and Normalized Cross-Correlation Values for ARFI Images in Fig. 4

	Axial Displacement (μm)			Normalized Cross-Correlation		
	Proximal Wall	**Distal Wall**	**Lumen**	**Proximal Wall**	**Distal Wall**	**Lumen**
4MHz Fundamental	0.83±0.45	0.81±0.47	3.14±3.15	0.997±0.005	0.999±0.002	0.973±0.041
8MHz Fundamental	0.69±0.48	0.92±1.02	3.73±3.65	0.994±0.008	0.996±0.006	0.944±0.076
Filtered Harmonic	0.93±1.07	0.73±0.38	7.06±6.44	0.991±0.013	0.997±0.003	0.863±0.143
PI (Fully Sampled) Harmonic	0.73±0.41	0.58±0.28	13.66±10.68	0.991±0.014	0.994±0.014	0.738±0.207